

Received: 20 December 2022

Revised: 27 January 2023

Accepted: 28 January 2023

Toward data- and mechanistic-driven volcano plots in electrocatalysis

Kai S. Exner^{1,2,3} ¹Faculty of Chemistry, Theoretical
Inorganic Chemistry, University
Duisburg-Essen, Essen, Germany²Cluster of Excellence RESOLV, Bochum,
Germany³Center for Nanointegration (CENIDE)
Duisburg-Essen, Duisburg, Germany

Correspondence

Kai S. Exner, University Duisburg-Essen,
Faculty of Chemistry, Theoretical
Inorganic Chemistry, Universitätsstraße 5,
45141 Essen, Germany.
Email: kai.exner@uni-due.deInvited contribution to the “From Spark
to Lightning” special issue of ELSA.

Funding information

Ministry of Culture and Science of the
Federal State of North Rhine-Westphalia,
Grant/Award Numbers: NRW Return
Grant, PI Exner; Deutsche
Forschungsgemeinschaft, Grant/Award
Numbers: EXC 2033 – 390677874 –
RESOLV, 388390466-TRR247

Abstract

The present application note summarizes an advanced methodology that allows for deriving potential-dependent volcano curves for energy storage and conversion processes. The conventional approach relies on the combination of density functional theory calculations and scaling relations for a single mechanistic pathway as well as a discussion of electrocatalytic activity by means of the potential-determining step, determined at the equilibrium potential of the reaction. Herein, it is illustrated how several reaction mechanisms can be factored into the volcano curve and how the rate-determining step based on the descriptor $G_{\max}(U)$ can be derived by a rigorous thermodynamic analysis of adsorption free energies fed by a data-inspired methodology.

KEYWORDS

data-driven approaches, descriptor-based analysis, electrocatalysis, potential-determining step, rate-determining step, volcano plot

1 | INTRODUCTION

Electrocatalysis has attributed a central role in the scenario of a sustainable energy economy, following the idea that energy production from intermittent renewables can be stored in chemical bonds without the depletion of nonrenewable resources.^[1–3] Important electrochemical devices for energy storage and conversion are electrolyzers to produce the energy vector gaseous hydrogen (H_2), fuel cells, and various types of batteries, ranging from lithium-based to post-lithium approaches or air-based and sulfur-based batteries.^[4–7] The electrochemical processes taking place at the electrodes in these devices are, however, neither

entirely understood relating to their mechanistic picture nor fully optimized for a large-scale operation in terms of cost-effectiveness, considering that these electrodes are often coated with scarce noble metals such as platinum, iridium, or ruthenium serving as the electrocatalyst.^[8,9] A major challenge in this field refers to the identification of economical electrocatalysts consisting of earth-abundant elements that have the potential to replace platinum- or iridium-based materials in fuel cells and electrolyzers in the long run.^[10–12]

While the theoretical description of electrocatalytic processes is inherently complex by considering the dynamic nature of the aqueous electrolyte, the occurrence of

This is an open access article under the terms of the [Creative Commons Attribution](https://creativecommons.org/licenses/by/4.0/) License, which permits use, distribution and reproduction in any medium, provided the original work is properly cited.

© 2023 The Authors. *Electrochemical Science Advances* published by Wiley-VCH GmbH.

adsorption and desorption processes on the electrode, and the presence of coupled or decoupled electron-proton or electron-cation transfer steps within multi-step reaction mechanism, it is noteworthy that in the last decade, theory has made major contributions relating to the identification of material motifs for electrocatalytic processes.^[13–15] Most of these works rely on the methodology introduced by Koper or Nørskov, Rossmeisl, and coworkers in that the binding energies of adsorbates on electrode surfaces are determined by density functional theory (DFT) calculations and are analyzed by the framework of scaling relations to construct volcano plots, which enable differentiation between active and inactive electrocatalyst.^[16–19] With the rise of artificial intelligence (AI) and machine-learning approaches, material optimization for thousands of potential material motifs can be performed by the volcano curve as a guideline, aiming to climb the volcano apex to reach superb electrocatalytic activity.^[20,21] While this procedure has been firmly established in the theoretical electrocatalysis community, I would like to outline the disadvantages of this method. On the one hand, the construction of volcano plots by using scaling relations commonly relies on the assumption of a single reaction mechanism, for instance, the mononuclear description via the *OH, *O, and *OOH adsorbates for the oxygen evolution or reduction reactions.^[22] Presuming a single reaction mechanism for all materials in a homologous series is yet a major restraint because this precondition is likely not met.^[23] On the other hand, the volcano legs are based on the determination of the so-called potential-determining step (PDS), which refers to the limiting reaction step in the thermodynamic picture at the equilibrium potential of the reaction. It has been demonstrated though that the PDS may not coincide with the rate-determining step (RDS) which governs electrocatalytic activity, and thus, the prediction of electrocatalytic activity based on the concept of PDS may be erroneous.^[24,25] Also, the applied overpotential, serving as the driving force for an electrocatalytic process, has a non-negligible impact on the location of the volcano apex, considering that an increase in the applied overpotential can displace the volcano top toward stronger or weaker bonding of a reaction intermediate.^[26–28]

In the present application note, I summarize a technique that has been recently established in my lab.^[29–33] There, we make use of a different strategy in that we do not follow the conventional scheme of DFT followed by scaling relations and volcano plots based on the PDS for a single reaction mechanism, and AI or data-science techniques to steer electrocatalytic activity, but rather we start from the opposite side: we make use of the already known scaling relations from literature and first, we describe a variety of mechanistic pathways by a rigorous thermodynamic treatment. Linking this thermodynamic analysis to

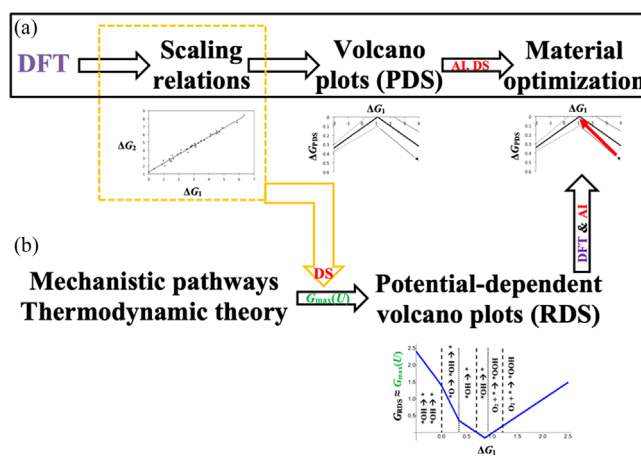


FIGURE 1 (a) Conventional approach in the literature for materials optimization (framed by a black box): density functional theory (DFT) calculations are conducted to derive scaling relations that translate to a volcano plot for a single reaction mechanism, discussing the potential-determining step (PDS) as activity descriptor. Artificial intelligence (AI) or data-science (DS) techniques are commonly applied for materials optimization to obtain catalysts with higher intrinsic activity in the approximation of the PDS. (b) Method derived in the Exner lab: instead of applying DFT calculations first, a variety of potential mechanistic descriptions are assessed by rigorous thermodynamic analysis, and the thermodynamic theory is linked with the already existing scaling relations from the literature and the activity descriptor $G_{\max}(U)$ by a data-science (DS) approach to obtain potential-dependent volcano plots, thereby discussing the free-energy span of $G_{\max}(U)$ referring to the rate-determining step (RDS) as activity descriptor. Thereafter, DFT calculations or AI can be used to conduct materials optimization based on the enhanced mechanistic picture of the volcano curve.

the descriptor $G_{\max}(U)$ ^[34,35] enables factoring overpotential and kinetic effects into the analysis to identify limiting reaction steps that scale with the RDS rather than the PDS, and the available material space is defined by a basis set of adsorption free energies. Our data-inspired methodology culminates into the construction of potential-dependent volcano curves, which can be compiled at any arbitrarily chosen overpotential, and thus may serve as a guideline for subsequent DFT calculations or AI investigations to optimize electrode materials. A summary of this approach is given in Figure 1.

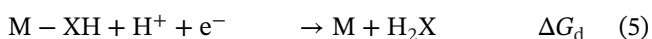
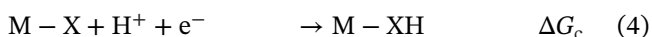
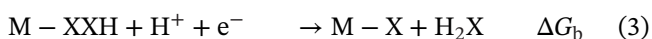
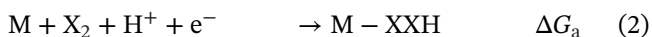
2 | MATHEMATICAL ORIGIN OF DATA-DRIVEN VOLCANO PLOTS

In the following, the scheme of Figure 1 is further explained with a general example. Let us assume a proton-electron coupled mechanism of reactant X_2 (for instance, O_2 or N_2 relating to the oxygen reduction or nitrogen

reduction reactions, respectively) to form the desired product, e. g., $2\text{H}_2\text{X}$:



In the first step, potential mechanistic pathways are formulated for the above reaction. While electrochemical reactions may contain both electrochemical and chemical steps, let us start the discussion with a mechanism where all steps are of electrochemical nature (cf. Equations (2)–(5)):



In Equations (2)–(5), the four free-energy changes relating to the elementary steps of the mechanism are indicated by ΔG_X ($X = a, b, c, d$). The sum of these four free-energy changes needs to fulfill the criterion of Equation (6), considering the fundamental laws of equilibrium thermodynamics:

$$\Delta G_a + \Delta G_b + \Delta G_c + \Delta G_d = -4 \cdot e \cdot U_{\text{X}_2/\text{H}_2\text{X}}@U = 0 \text{ vs. RHE} \quad (6)$$

Consequently, the free-energy change ΔG_d can always be referred to as Equation (6) so that only the free-energy changes ΔG_a , ΔG_b , and ΔG_c are independent variables. One of these free-energy changes is used as a descriptor in the volcano analysis, e. g., ΔG_a . The free-energy changes ΔG_b and ΔG_c are correlated by scaling relations to the descriptor ΔG_a , as exemplified by Equations (7) and (8):

$$\Delta G_b = f_1(\Delta G_a, \text{SR1}) \quad (7)$$

$$\Delta G_c = f_2(\Delta G_a, \text{SR2}) \quad (8)$$

Here, SR1 and SR2 denote two different scaling relations that connect the respective free-energy change to the descriptor ΔG_a . The scaling relations SR1 and SR2 can be taken from the literature and can also be treated as data ranges in that one is studying the impact of a varying scaling relation on the volcano curve.^[29,30] Applying the outlined procedure, only one (ΔG_a) of the initial four

free-energy changes (cf. Equations (2)–(5)) remains as a variable in the analysis. This variable serves as a descriptor

in the volcano approach, for which a data range is defined that represents the material space, thereby referring to DFT studies from the literature.^[31–33]

In the next step, the free energies of the reaction intermediates of the mechanistic description in Equations (2)–(5) are expressed by means of the above free-energy changes:

$$G_{\text{M}+\text{X}_2}(U) = 0 \quad (9)$$

$$G_{\text{M}-\text{XXH}}(U) = \Delta G_a + 1 \cdot e \cdot U \quad (10)$$

$$G_{\text{M}-\text{X}}(U) = \Delta G_a + \Delta G_b + 2 \cdot e \cdot U \quad (11)$$

$$G_{\text{M}-\text{XH}}(U) = \Delta G_a + \Delta G_b + \Delta G_c + 3 \cdot e \cdot U \quad (12)$$

$$G_{\text{M}+\text{H}_2\text{X}}(U) = \Delta G_a + \Delta G_b + \Delta G_c + \Delta G_d + 4 \cdot e \cdot U \quad (13)$$

By referring to the above discussion, we can replace ΔG_b , ΔG_c , and ΔG_d with the scaling relations or the equilibrium potential, respectively:

$$G_{\text{M}+\text{X}_2}(U) = 0 \quad (14)$$

$$G_{\text{M}-\text{XXH}}(U) = \Delta G_a + 1 \cdot e \cdot U \quad (15)$$

$$G_{\text{M}-\text{X}}(U) = \Delta G_a + f_1(\Delta G_a, \text{SR1}) + 2 \cdot e \cdot U \quad (16)$$

$$G_{\text{M}-\text{XH}}(U) = \Delta G_a + f_1(\Delta G_a, \text{SR1}) + f_2(\Delta G_a, \text{SR2}) + 3 \cdot e \cdot U \quad (17)$$

$$G_{\text{M}+\text{H}_2\text{X}}(U) = -4 \cdot e \cdot U_{\text{X}_2/\text{H}_2\text{X}} + 4 \cdot e \cdot U \quad (18)$$

To approximate electrocatalytic activity and to identify limiting reaction steps, we do not apply the concept of PDS, but rather make use of the descriptor $G_{\text{max}}(U)$ ^[34,35] that relies on the idea of a free-energy span model by ana-

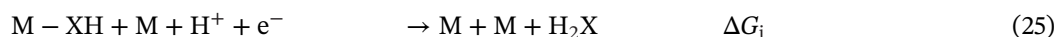
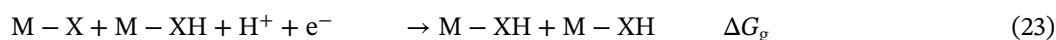
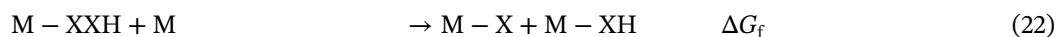
lyzing all possible free-energy spans between the reaction intermediates^[36,37]:

$$\begin{aligned} &G_{M-XXH}(U) - G_{M+X_2}(U); G_{M-X}(U) - G_{M+X_2}(U); G_{M-XH}(U) - G_{M+X_2}(U); \\ &G_{M-X}(U) - G_{M-XXH}(U); G_{M-XH}(U) - G_{M-XXH}(U); G_{M+H_2X}(U) - G_{M-XXH}(U); \\ &G_{M-XH}(U) - G_{M-X}(U); G_{M+H_2X}(U) - G_{M-X}(U); G_{M+H_2X}(U) - G_{M-XH}(U) \end{aligned} \quad (19)$$

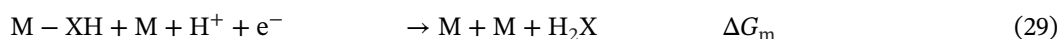
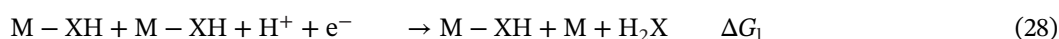
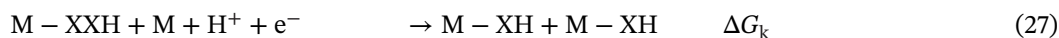
The largest free-energy difference among the set of available spans is extracted because this span has been shown to correlate with the RDS of the overall reaction^[34,35]:

$$\begin{aligned} G_{\max}(U) = \max\{ &G_{M-XXH}(U) - G_{M+X_2}(U); G_{M-X}(U) - G_{M+X_2}(U); G_{M-XH}(U) - G_{M+X_2}(U); \\ &G_{M-X}(U) - G_{M-XXH}(U); G_{M-XH}(U) - G_{M-XXH}(U); G_{M+H_2X}(U) - G_{M-XXH}(U); \\ &G_{M-XH}(U) - G_{M-X}(U); G_{M+H_2X}(U) - G_{M-X}(U); G_{M+H_2X}(U) - G_{M-XH}(U) \} \end{aligned} \quad (20)$$

The procedure of Equations (2–20) allows compiling a volcano curve for the electrocatalytic process of Equation (1) by varying the descriptor ΔG_a in its considered data range. This methodology, however, is not only carried out for the mechanistic pathway of Equations (2)–(5) but also for other conceivable mechanisms. For instance, another potential mechanism for the reaction of Equation (1) is reconciled with Equations (21)–(25):



A third option refers to Equation (26)–(29):



Here, I want to refrain from a long mathematical derivation of the reaction intermediates' energetics for the other

two mechanistic pathways because they can be found in previous publications of the author.^[38,39] The essence of this procedure refers to the combination of the volcano

curves for the dissimilar mechanisms into a single plot to identify the preferred mechanism and limiting steps depending on the descriptor ΔG_a .

While so far, the discussion relies on a general example of converting X_2 into an energetically favored product under the application of a cathodic potential, let us exemplify this framework by a concrete electrocatalytic process. For the oxygen reduction reaction (ORR), X_2

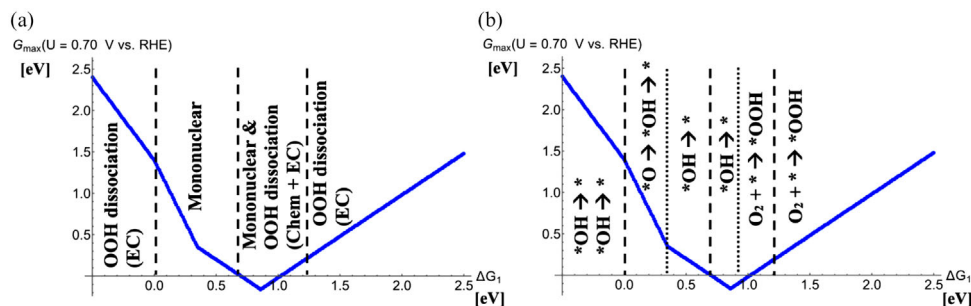


FIGURE 2 (a) Volcano plot of the mononuclear, chemical *OOH dissociation, and electrochemical *OOH dissociation mechanisms with a scaling-relation intercept of 3.2 eV for the four-electron oxygen reduction reaction at $U = 0.7$ V versus reversible hydrogen electrode (RHE). The energetically favored pathway in each regime of the descriptor ΔG_1 is indicated. (b) Limiting reaction steps based on the free-energy span of $G_{\max}(U = 0.7$ V vs. RHE) for the respective mechanism in dependence of ΔG_1 . Panel (a) is adopted with permission.^[39]

refers to O_2 , U_{X_2/H_2X} amounts to 1.23 V versus reversible hydrogen electrode (RHE), and the mechanistic pathways of Equations (2)–(5), (21)–(25), and (26)–(29) are reconciled with the mononuclear, chemical OOH dissociation, and electrochemical OOH dissociation mechanisms, respectively.^[40–44] Relating to the descriptor ΔG_a , the adsorption-free energy of the *OH adsorbate, ΔG_1 , is chosen, corresponding to the reverse reaction of Equation (5). Two scaling relations are considered, namely the adsorption-free energy of the *O adsorbates is about twice the *OH intermediate, and the *OOH and *OH adsorbates scale with an offset of about 3.2 eV.^[17,18] Given that basically all relevant materials to the oxygen electrocatalysis are within $\Delta G_1 = [-0.50, 2.50]$ eV,^[45] this value range is used to derive the volcano curve using $G_{\max}(U = 0.7$ V vs. RHE) as activity descriptor on the y axis. The obtained results are depicted in Figure 2.

Figure 2a illustrates that in different regimes of the descriptor ΔG_1 , dissimilar mechanistic descriptions are energetically preferred, and thus govern activity in the volcano curve. While for strong and weak binding of the *OH adsorbate, the OOH dissociation mechanism controls the shape of the volcano curve, the mononuclear mechanism is preferred for $0 \text{ eV} < \Delta G_1 < 0.7 \text{ eV}$. Near or at the volcano top ($0.8 \text{ eV} < \Delta G_1 < 1.2 \text{ eV}$), however, all three mechanisms compete. This finding illustrates that highly active ORR catalysts benefit from the fact that not only one pathway is operative, but rather these catalysts have the advantage of reducing O_2 to water via different mechanisms. Though, so far, it is common consensus to the approximate activity of highly active ORR catalysts by testing a single mechanistic description,^[38,40] which, based on the derived volcano curve, is too simplistic.

Figure 2b indicates the limiting reaction steps in the framework of $G_{\max}(U = 0.7$ V vs. RHE). It becomes evident that the limiting steps alter when the preferred mechanism switches from the OOH dissociation to the mononuclear description ($\Delta G_1 = 0$ eV). On the other

hand, it turns out that the limiting step can even be changed in the free-energy regime of $0 \text{ eV} < \Delta G_1 < 0.7 \text{ eV}$ where the mononuclear mechanism is operative: while the free-energy span $G_M(U) - G_{M-O}(U)$ governs $G_{\max}(U)$ for $\Delta G_1 < 0.35$ eV, its definition is given by the free-energy difference $G_M(U) - G_{M-OH}(U)$ for $\Delta G_1 > 0.35$ eV. The observed change in the intermediate states governing $G_{\max}(U)$ cannot be resolved by the conventionally applied PDS concept in volcano plots but rather requires a potential-dependent contemplation of the intermediate states by the free-energy span model, which can also be linked to the RDS if the Tafel slope is predetermined. Given that for overpotentials exceeding 500 mV, it can be fairly assumed that the first electrochemical step in the mechanism (Tafel slope of 120 mV/dec) governs the rate,^[34] the different free-energy spans translate to a dissimilar RDS at $U = 0.7$ V versus RHE, namely either $*O \rightarrow *OH$ or $*OH \rightarrow *$ for $\Delta G_1 < 0.35$ eV and $\Delta G_1 > 0.35$ eV, respectively. Further discussion on the U -dependence of the ORR volcano plot based on the outlined methodology is given.^[38,39]

The above example illustrates that, without any ado, the commonly made assumption that the limiting step is not altered at the volcano legs does not hold true, which is reminiscent of the discussion of Schmickler and coworkers in reference.^[46] Additionally, it is noteworthy that the consideration of an insufficient number of mechanisms in the approach can lead to an underestimation of electrocatalytic activity because in this case, the volcano curve traces the electrocatalytic activity to a mechanism that is not reconciled with the energetically favored pathway. These findings underpin the importance of the advanced volcano methodology based on the introduced scheme in Figure 1.

For the volcano curve of Figure 2, subsequently, DFT calculations can be applied for potential ORR electrocatalysts to categorize these materials into active and inactive and to quantify limiting reaction steps based on the preferred mechanistic description. Similar to the conventional

approach, the volcano plot also allows the optimization of materials with AI and data-science techniques by relying on a different optimization scheme in that limiting steps in the framework of the descriptor $G_{\max}(U)$ rather than the PDS are discussed (cf. Figure 1). The outlined concept is universal and can therefore be applied to any proton-electron transfer process of relevance to energy storage and conversion, for which adsorption-energy scaling relations are already available.^[47] Besides the ORR,^[38,39] further examples in the literature comprise nitrogen reduction,^[31,32] oxygen evolution,^[30,33] and bifunctional oxygen electrocatalysis^[29] to which the interested reader is referred.

3 | CONCLUSIONS

Materials optimization for electrocatalytic processes has been largely governed by a combination of DFT calculations to derive scaling relations and volcano plots. While these considerations largely neglect the opportunity of several mechanistic pathways in the analysis and are based on a simplified description of electrocatalytic activity by relying on thermodynamic considerations in terms of the potential-determining step (PDS), the present application note summarizes an advanced framework that goes beyond volcano curves for a single mechanism and the PDS as activity descriptor. Combining scaling relations from the literature with a rigorous thermodynamic treatment of various mechanistic pathways and a potential-dependent activity descriptor, $G_{\max}(U)$, volcano plots are derived that allow unraveling mechanistic changes as well as switches in the limiting steps referring to the RDS rather than the PDS. Due to the universality of the introduced methodology, I am confident that the outlined procedure not only enhances our atomic scale understanding of electrocatalytic processes but also contributes to the design of catalytic materials for energy conversion and storage processes.

ACKNOWLEDGEMENTS

Kai S. Exner acknowledges funding from the Ministry of Culture and Science of the Federal State of North Rhine-Westphalia (NRW Return Grant, PI Exner). Kai S. Exner is associated with the CRC/ TRR247: “Heterogeneous Oxidation Catalysis in the Liquid Phase” (Project number 388390466-TRR 247), the RESOLV Cluster of Excellence, funded by the Deutsche Forschungsgemeinschaft under Germany’s Excellence Strategy—EXC 2033 – 390677874 – RESOLV, and the Center for Nanointegration (CENIDE). This article is based upon the work from COST Action 18234, supported by COST (European Cooperation in Science and Technology).

CONFLICT OF INTEREST STATEMENT

The authors declare no conflict of interest.

DATA AVAILABILITY STATEMENT

Not Applicable.

ORCID

Kai S. Exner  <https://orcid.org/0000-0003-2934-6075>

REFERENCES

- Z. W. Seh, J. Kibsgaard, C. F. Dickens, I. Chorkendorff, J. K. Nørskov, T. F. Jaramillo, *Science* **2017**, 355, eaad4998.
- J. J. Sirola, *Curr. Opin. Chem. Eng.* **2014**, 5, 96.
- G. W. Crabtree, M. S. Dresselhaus, M. V. Buchanan, *Phys. Today* **2004**, 57, 39.
- M. Carmo, D. L. Fritz, J. Mergel, D. Stolten, *Int. J. Hydrog. Energy* **2013**, 38, 4901.
- A. A. Gewirth, J. A. Varnell, A. M. DiAscro, *Chem. Rev.* **2018**, 118, 2313.
- J. Janek, W. G. Zeier, *Nat. Energy* **2016**, 1, 16141.
- P. G. Bruce, S. A. Freunberger, L. J. Hardwick, J.-M. Tarascon, *Nat. Mater.* **2012**, 11, 19.
- C. Y. Wang, *Chem. Rev.* **2004**, 104, 4727.
- J. Kibsgaard, I. Chorkendorff, *Nat. Energy* **2019**, 4, 430.
- H. Yang, J. N. Hausmann, V. Hlukhyy, T. Braun, K. Laun, I. Zebger, M. Driess, P. W. Menezes, *Chem. Cat. Chem.* **2022**, 14, e202200293.
- J. Kibsgaard, Z. Chen, B. N. Reinecke, T. F. Jaramillo, *Nat. Mater.* **2012**, 11, 963.
- J. Song, C. Wei, Z.-F. Huang, C. Liu, L. Zeng, X. Wang, Z. J. Xu, *Chem. Soc. Rev.* **2020**, 49, 2196.
- J. Greeley, T. F. Jaramillo, J. Bonde, I. Chorkendorff, J. K. Nørskov, *Nat. Mater.* **2006**, 5, 909.
- D. Voiry, H. Yamaguchi, J. Li, R. Silva, D. C. B. Alves, T. Fujita, M. Chen, T. Asefa, V. B. Shenoy, G. Eda, M. Chhowalla, *Nat. Mater.* **2013**, 12, 850.
- Z. W. Seh, K. D. Fredrickson, B. Anasori, J. Kibsgaard, A. L. Strickler, M. R. Lukatskaya, Y. Gogotsi, T. F. Jaramillo, A. Vojvodic, *ACS Energy Lett.* **2016**, 1, 589.
- J. K. Nørskov, J. Rossmeisl, A. Logadottir, L. Lindqvist, J. R. Kitchin, T. Bligaard, H. Jónsson, *J. Phys. Chem. B.* **2004**, 108, 17886.
- I. C. Man, H.-Y. Su, F. Calle-Vallejo, H. A. Hansen, J. I. Martinez, N. G. Inoglu, J. Kitchin, T. F. Jaramillo, J. K. Nørskov, J. Rossmeisl, *Chem. Cat. Chem.* **2011**, 3, 1159.
- M. T. M. Koper, *J. Electroanal. Chem.* **2011**, 660, 254.
- M. T. M. Koper, *Chem. Sci.* **2013**, 4, 2710.
- S. Back, J. Yoon, N. Tian, W. Zhong, K. Tran, Z. W. Ulissi, *J. Phys. Chem. Lett.* **2019**, 10, 4401.
- S. Back, K. Tran, Z. W. Ulissi, *ACS Catal.* **2019**, 9, 7651.
- D. Antipin, M. Risch, *Electrochem. Sci. Adv.* **2022**, <https://doi.org/10.1002/elsa.202100213>
- L. Zhong, S. Li, *ACS Catal.* **2020**, 10, 4313.
- M. T. M. Koper, *J. Solid State Electrochem* **2013**, 17, 339.
- K. S. Exner, *ACS Catal.* **2019**, 9, 5320.
- K. S. Exner, *Angew. Chem. Int. Ed.* **2020**, 59, 10236.
- H. Ooka, R. Nakamura, *J. Phys. Chem. Lett.* **2019**, 10, 6706.
- Y. Zhang, J. Zhang, J. Huang, *J. Phys. Chem. Lett.* **2019**, 10, 7037.

29. S. Razzaq, K. S. Exner, *Chem. Electro. Chem.* **2022**, *9*, e202101603.
30. S. Razzaq, K. S. Exner, *Electrochim. Acta.* **2022**, *412*, 140125.
31. K. S. Exner, *Chin. J. Catal.* **2022**, *43*, 2871.
32. K. S. Exner, *Chem. Cat. Chem.* **2022**, *14*, e2022003666.
33. K. S. Exner, *Phys. Energy* **2023**, *5*, 014008.
34. K. S. Exner, *ACS Catal.* **2020**, *10*, 12607.
35. K. S. Exner, *Electrochim. Acta.* **2021**, *375*, 137975.
36. S. Kozuch, S. Shaik, *Acc. Chem. Res.* **2011**, *44*, 101.
37. J. Chen, Y. Chen, P. Li, Z. Wen, S. Chen, *ACS Catal.* **2018**, *8*, 10590.
38. K. S. Exner, *Chem. Cat. Chem.* **2022**, e202201222.
39. K. S. Exner, *ACS Phys. Chem. Au.* **2023**, <https://doi.org/10.1021/acspchemau.2c00054>
40. V. Viswanathan, H. A. Hansen, J. Rossmeisl, J. K. Nørskov, *ACS Catal.* **2012**, *2*, 1654.
41. X. Ge, A. Sumboja, D. Wu, T. An, B. Li, F. W. T. Goh, T. S. A. Hor, Y. Zong, Z. Liu, *ACS Catal.* **2015**, *5*, 4643.
42. A. Kulkarni, S. Siahrostami, A. Patel, J. K. Nørskov, *Chem. Rev.* **2018**, *118*, 2302.
43. L. Yu, X. Pan, X. Cao, X. Bao, *J. Catal.* **2011**, *282*, 183.
44. J. Huang, J. Zhang, M. Eikerling, *Phys. Chem. Chem. Phys.* **2018**, *20*, 11776.
45. S. Divanis, T. Kutlusoy, I. M. I. Boye, I. C. Man, J. Rossmeisl, *Chem. Sci.* **2020**, *11*, 2943.
46. P. Quaino, F. Juarez, E. Santos, W. Schmickler, *Beilstein J. Nanotechnol.* **2014**, *5*, 846.
47. S. Razzaq, K. S. Exner, *ACS Catal.* **2023**, *13*, 1740.

How to cite this article: K. S. Exner, *Electrochem Sci Adv.* **2024**, *4*, e2200014.
<https://doi.org/10.1002/elsa.202200014>

DuEPublico

Duisburg-Essen Publications online

UNIVERSITÄT
DUISBURG
ESSEN

Offen im Denken

ub | universitäts
bibliothek

This text is made available via DuEPublico, the institutional repository of the University of Duisburg-Essen. This version may eventually differ from another version distributed by a commercial publisher.

DOI: 10.1002/elsa.202200014

URN: urn:nbn:de:hbz:465-20240418-090828-4



This work may be used under a Creative Commons Attribution 4.0 License (CC BY 4.0).